

Observations and Variability of Near-Surface Atmospheric Electric Fields across Multiple Stations

Wen Li ^{1,2}, Zhibin Sun ^{1,*}, Zhaoai Yan ¹ and Zhongsong Ma ³

¹ State Key Laboratory of Space Weather, National Space Science Center, Chinese Academy of Sciences, Beijing 100190, China; liwen@nssc.ac.cn (W.L.); yanza@126.com (Z.Y.)

² University of Chinese Academy of Sciences, Beijing 100049, China

³ Technology and Engineering Center for Space Utilization, Chinese Academy of Sciences, Beijing 100094, China; mazhongsong@csu.ac.cn

* Correspondence: zbsun@nssc.ac.cn; Tel.: +86-138-1019-5052

Abstract: The near-surface atmospheric electrostatic field plays a pivotal role in comprehending the global atmospheric circuit model and its influence on climate change. Prior to delving into the intricate interplay between solar activities, geological activities, and atmospheric electric field, a comprehensive examination of the diurnal fair atmospheric electric field's baseline curve within a specific region is essential. Based on the atmospheric electric field network monitoring in Yunnan Province in the year 2022, this study systematically investigated the distribution of the atmospheric electric field under both fair-weather and disturbed weather conditions at a quadrilateral array encompassing Chuxiong Station, Mouding Station, Lufeng Station, and Dali Station. The primary focus was on elucidating the variations in the daily variation curves of fair atmospheric electric fields and conducting a comparative analysis with the Carnegie curves. The possible reasons for the differences among them are also discussed in this study, but more observational evidence is required to confirm the specific causes in the future.

Keywords: near-surface observations; atmospheric electric field; variability; multiple stations



Citation: Li, W.; Sun, Z.; Yan, Z.; Ma, Z. Observations and Variability of Near-Surface Atmospheric Electric Fields across Multiple Stations. *Atmosphere* **2024**, *15*, 124. <https://doi.org/10.3390/atmos15010124>

Academic Editor: Sergey Pulintsev

Received: 19 December 2023

Revised: 15 January 2024

Accepted: 18 January 2024

Published: 19 January 2024



Copyright: © 2024 by the authors. Licensee MDPI, Basel, Switzerland. This article is an open access article distributed under the terms and conditions of the Creative Commons Attribution (CC BY) license (<https://creativecommons.org/licenses/by/4.0/>).

1. Introduction

The near-surface atmospheric electric field (AEF) is a fundamental and vital variable in atmospheric electricity [1,2], which reflects distribution status of atmospheric static charges in the surrounding environment. In addition, it serves as a crucial foundation for studying solar activities, understanding the relationship between global atmospheric circuit models and climate change, monitoring earthquake precursors [3–12], and issuing of thunderstorm warnings [13–15]. Wilson et al. [16] proposed a global atmospheric circuit model in 1921, highlighting that the intensity of fair-weather atmospheric electric fields is influenced not only by underground radioactive materials such as radon but also by galactic cosmic rays, solar cosmic rays, relativistic electrons, and solar activity [17–21]. These influencing factors can modify atmospheric conductivity and the AEF by modulating the ionization rate of the global atmosphere.

It is widely recognized that the near-surface AEF exerts both local and global effects. Before investigating the impact of specific factors on near-surface atmospheric electricity, it is imperative to first examine the baseline curve of the diurnal fair atmospheric electric field in a given region. The Carnegie Institute [22] conducted measurements of the daily variation curve of the AEF over the ocean, which is regarded as the global average daily variation. This curve demonstrates a peak value near 19 UT and a minimum value close to 3 UT. During the observation period, when there is no daily variation in convection over the ocean, the daily variations in the AEF align with the daily variations in ionospheric potential, known as the “Carnegie curve”. This curve serves as a valuable reference for comparing daily variation curves of fair-weather AEFs in different regions.

Numerous scholars have extensively studied the diurnal variations in the near-surface AEF under different weather conditions. Bhattacharyya et al. [23] investigated fair-weather AEFs at high-altitude stations in the eastern Himalayas during 2017–2018. Upon comparing the local average fair-weather AEF curve with the Carnegie curve, they observed that the local AEF values at high altitudes generally exceeded the Carnegie curve. These differences exhibited a strong correlation with local meteorological parameters and the atmospheric composition. Additionally, Li et al. [24] compiled a dataset of fair-weather AEFs at the Zhongshan Chinese Antarctic Station and Beijing Changping Station from 1 March 1 to 1 August 2022. The results revealed a more complex average daily variation in the fair-weather AEF in Beijing compared to Antarctica. The average fair-weather AEF value in Antarctica was significantly higher than that in Beijing by 370 V/m. Consequently, Li et al. [25] conducted a detailed discussion on the reasons for these differences. They utilized AEF datasets and meteorological data, including relative humidity, wind speed, precipitation, and visibility, at Gar Station (80.13° E, 32.52° N, 4259 m above sea level) on the Tibetan Plateau during November 2021 to October 2022. Their study focused on minutely analyzing the effects of various meteorological parameters on the AEF and summarizing the ideal fair-weather conditions for the AEF without meteorological disturbances at Gar Station. Furthermore, Wu et al. [26] delved into the characteristics of near-surface AEFs under different weather conditions in Beijing. They analyzed data collected from the roof of the Physics Building of Peking University between August 2004 and November 2005. Their findings indicated that the fair-weather average AEF variation curves in Beijing exhibited “double peaks, double valleys,” with valleys occurring at 05:00 and 12:00 (local time, UTC+8) and peaks at 07:00 and 23:00 (local time, UTC+8).

Considering that differences in geological structures among different regions can significantly impact the distribution of atmospheric static charges, establishing multiple AEF observation stations in the same area allows for more effective comparisons. Thus, the researchers established a quadrilateral AEF observation network in the region in order to investigate the local effects of the near-surface AEF in Yunnan (a province of China). The aim was to unveil the potential local factors influencing the AEF by analyzing the differences in diurnal variations among these stations. This paper focuses on the quadrilateral AEF observation network, examining the distribution of fair-weather AEF data at the four stations in 2022, comparing the AEF distributions under both fair and disturbed weather conditions, and analyzing variations in fair-weather AEF curves compared to the standard Carnegie curve.

2. Observations

Yunnan, situated inland and surrounded by high mountains, is far from the ocean, making it an ideal location for establishing a specialized physics experimental field. Recognizing the potential for comparing various AEF values across different regions using multiple stations, researchers have developed a quadrilateral monitoring network comprising four AEF stations around Kunming in Yunnan Province. These long-term observations have been conducted since the year 2020 and continue to the present. The four stations include Chuxiong (CX) Station (101.58° E, 24.93° N, 1781 m above mean sea level (amsl)), Mouding (MD) Station (101.44° E, 25.36° N, 1777 m amsl), Lufeng (LF) Station (102.27° E, 25.39° N, 1634 m amsl), and Dali (DL) Station (100.18° E, 25.71° N, 1360 m amsl). Their locations are illustrated in Figure 1, where the colors (from brown to yellow) denote different altitudes (amsl) and the four blue triangles indicate the positions of the AEF observation stations. Notably, the stations exhibit similar altitudes, with DL Station at the highest altitude and LF Station at the lowest.

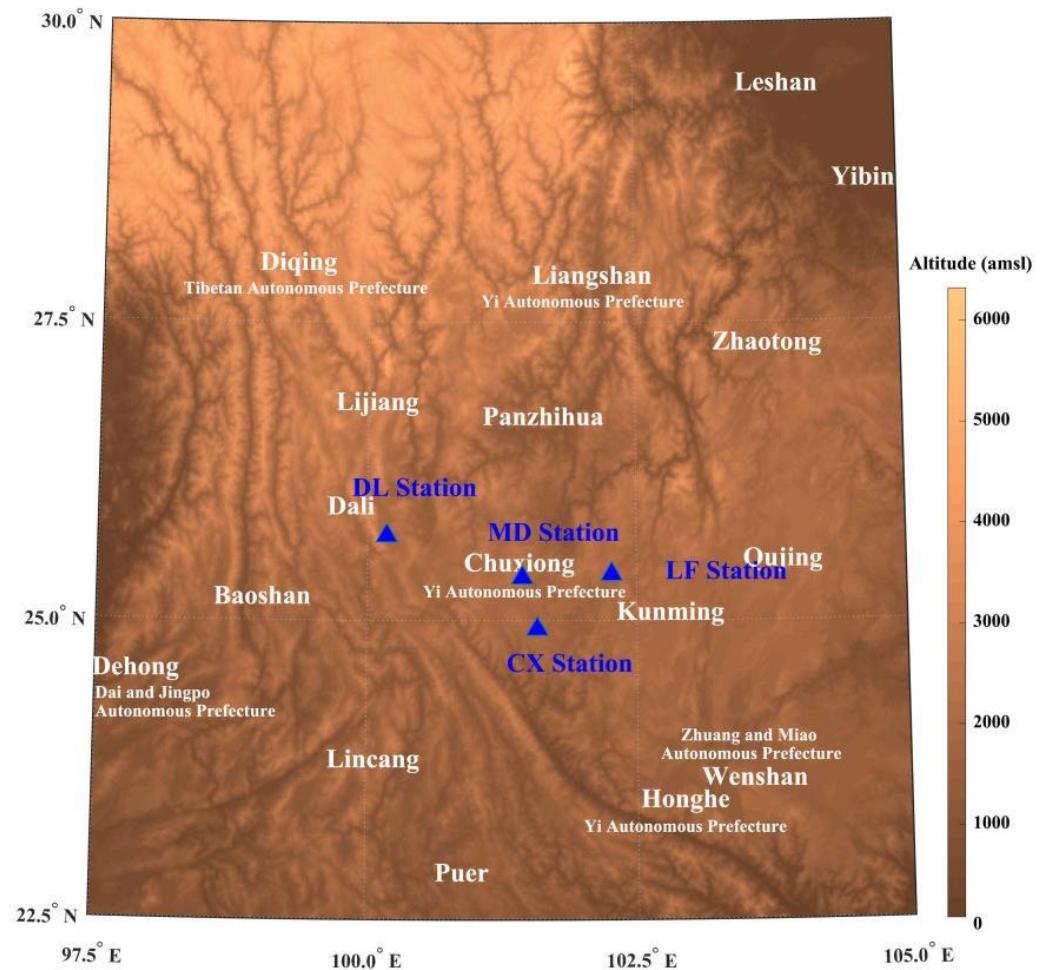


Figure 1. Atmospheric electric field stations map (brown to yellow colors denote different altitudes, blue triangles indicate the four stations).

The instruments employed for measuring the surface AEF at the four stations include EFM 100s (A type of AEF meter) [24], characterized by a measurement range of ± 50 kV/m, measurement accuracy below 5%, and a resolution of 10 V/m. These instruments are solar-powered on fair days and equipped with batteries for storing electricity in overcast conditions when sunlight is insufficient. A real-time transmission of AEF data is facilitated through the 4G telephone network, with an AEF value measured every second. Figure 2 illustrates the schematic diagram of the EFM 100 probe, which includes a DC motor, motor control circuit, preamplifier, grounding brush, insulated connecting rod, stator, shell, and rotor. The DC motor is responsible for driving the rotor to rotate, and the motor control circuit controls both the DC motor and the preamplifier, which amplifies the DC current. The grounding brush ensures the conduction of current between the rotating and stationary components. The insulated connecting rod ensures that the stator remains ungrounded, while the rotor, connected through a central metal rod, is grounded. The stator generates induced charges, and the rotor, consisting of rotating metal blades, causes periodic changes in the exposed area of the stator, generating alternating currents. The stator and rotor are two sets of similarly shaped fan-shaped metal conductive plates. The stator, fixed on a support plate as the inductive plate (generating induced charges), and the rotor, driven by the motor and rotating at a constant speed as the shielding plate, are connected to the rotating metal rod, grounded together with the rotating blades. The stator is connected to the support plate through an insulated connecting rod. During normal operation, the motor drives the rotor to rotate at a constant speed. Each fan blade of the stator is periodically and alternately exposed to the ambient electric field, causing each fan

blade in the stator to generate induced charges and, consequently, producing an alternating current signal. Since the atmospheric static electric field is a DC component, the induced current on the inductive plate is very weak and needs to be amplified before atmospheric electric field measurements can be conducted. The preamplifier amplifies the weak current signal generated by induction. The signal then undergoes current–voltage conversion, amplification, filtering, signal synchronization, rectification, and other processes, resulting in an output voltage signal. Finally, through data processing and calculations, the desired atmospheric electric field data are obtained. The calibration of the EFM 100 probe is conducted indoors by placing the electric field probe in a calibration box. By applying a voltage to generate a simulated electric field, the probe is calibrated by comparing the numerical values of the simulated electric field with the measured values.

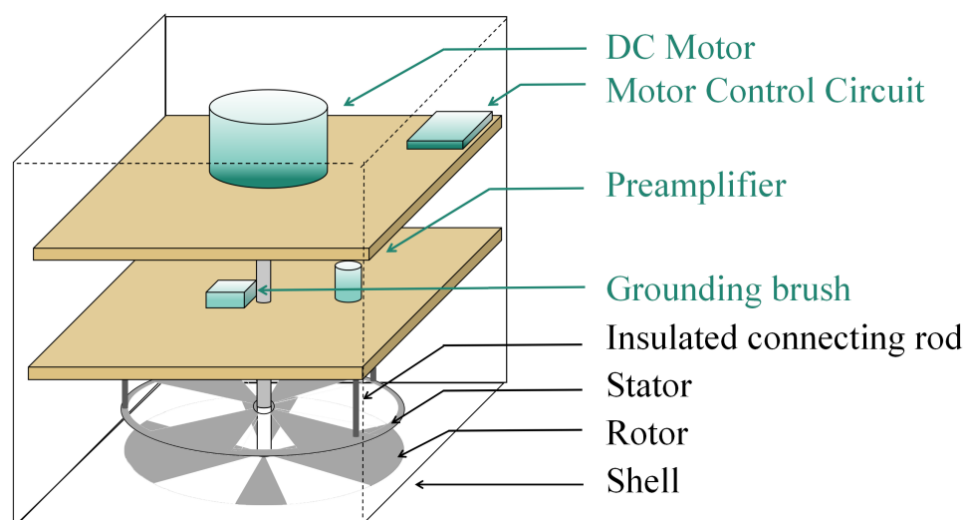


Figure 2. Schematic diagram of EFM 100's probe.

To ensure a clear distinction between fair-weather AEFs and disturbed-weather AEFs, it is crucial to establish a precise definition of fair weather, incorporating explicit quantitative criteria for unique determination and classification of fair days. This research adopted the fair-weather quantitative criteria detailed by Harrison and Nicoll [27], encompassing the following conditions: (1) absence of precipitation; (2) hourly average relative humidity not exceeding 95%; (3) surface hourly average wind speed not exceeding 7 m/s; and (4) AEF values ranging from 0 to 1 kV/m.

3. Results

Utilizing the aforementioned fair-weather criteria, Table 1 presents the count of different fair days across the various seasons and the number of valid days at CX Station, MD Station, LF Station, and DL Station. The first number represents fair days, while the number inside the brackets indicates valid days. It is important to note that invalid days refer to instances where AEF data were lost for more than 2 h. Upon examination of Table 1, LF Station exhibited the most significant data loss, whereas CX Station boasts the largest number of fair days. Notably, MD Station experienced the highest number of fine days during October–December, whereas DL Station recorded the fewest fair days from April to June. The data in Table 1 clearly illustrate that fair days are the least frequent during summer, with the highest occurrence observed in winter and spring, surpassing both autumn and summer for all four stations.

Table 1. Fair days and valid days (in brackets) at CX, MD, LF, and DL Stations in different seasons.

	CX Station	MD Station	LF Station	DL Station
January–March	69 (88)	58 (88)	15 (27)	25 (88)
April–June	57 (83)	38 (88)	3 (32)	2 (89)
July–September	43 (77)	37 (88)	10 (42)	65 (91)
October–December	67 (78)	75 (92)	66 (82)	40 (44)

The researchers delineated the distribution of fair-weather AEFs and disturbed-weather AEFs based on the established fair-weather discrimination criteria. The distributions for the year 2022 are depicted in Figure 3, where the left panel illustrates the AEF distribution in fair weather, while the right panel represents the AEF distribution under disturbed weather conditions. Various colors are employed to denote different stations, with blue diagonal lines indicating the AEF at CX Station, red diagonal lines representing the AEF at MD Station, green bars depicting the AEF for LF Station, and yellow bars indicating the AEF for DL Station. In Figure 3, the upper and lower boxes display the 90th, 75th, 15th, and 10th percentiles, respectively. The horizontal lines within the boxes represent the median AEF values, and the dashed lines denote an AEF value of 0 V/m. It is essential to note that the AEF data distribution in Figure 3 reflects 1 min averaged AEF values.

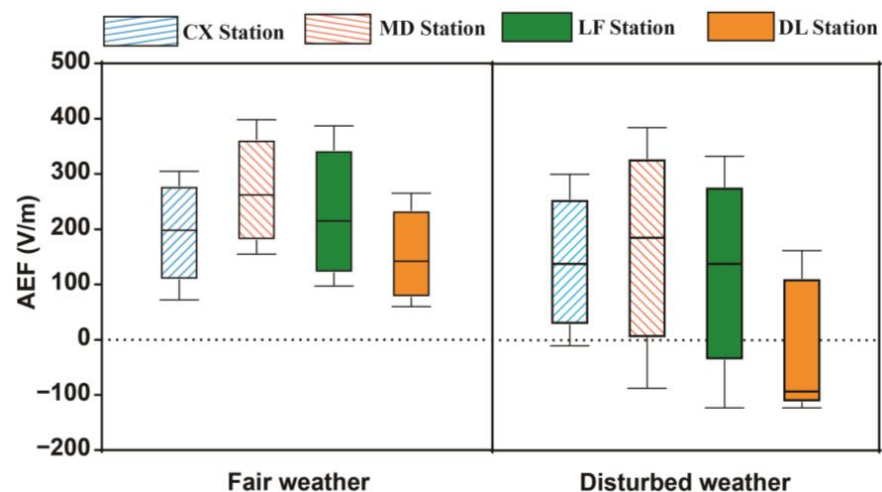


Figure 3. Distribution of fair-weather (left) and disturbed weather (right) AEFs in 2022 (upper and lower boxes indicate 90th, 75th, 15th, 10th percentiles, respectively, horizontal lines in boxes indicate median AEF values, and the dashed lines denote 0 V/m).

Under fair weather conditions, the median AEF values for all four stations ranged from 100 to 300 V/m. MD Station exhibited the highest median AEF at 262 V/m, while DL Station had the smallest value at 142 V/m. In terms of distribution ranges, MD and LF Stations demonstrated wider and higher AEF distributions compared to CX Station and DL Station. Similarly, under disturbed weather conditions, the results mirror those of the fair weather results. MD Station recorded the largest median AEF at 185 V/m, while DL Station had the smallest value at -93 V/m. Consequently, MD Station and LF Station exhibited a broader range of AEF distribution than the other stations. A comparison between the left and right panels in Figure 3 reveals that the distribution of the AEF under disturbed weather conditions was wider than that under fair weather conditions, and the AEF values under disturbed weather conditions were lower. This is attributed to the prevalence of more negative AEF values during disturbed weather, aligning with the conventional knowledge [28]. Additionally, DL Station displayed the narrowest distribution range among the four stations, correlating with its lowest altitude.

Figure 4 displays histograms illustrating the distribution of fair-weather AEF values at the four stations, offering a more detailed representation of the fair-weather AEF distribution. Panel (a) illustrates the histogram for CX Station, panel (b) depicts the distribution of fair-weather AEF values at MD Station, panel (c) represents LF Station, and panel (d) shows DL Station. The vertical axis indicates histogram density, while the horizontal axis denotes AEF ranges, with intervals of 10 V/m. It is important to note that the data distribution in Figure 4 represents values recorded every second and has not been treated. Additionally, values in the range of 400–500 V/m are all aggregated in the last histogram due to the limited range on the horizontal axis of the distribution figure.

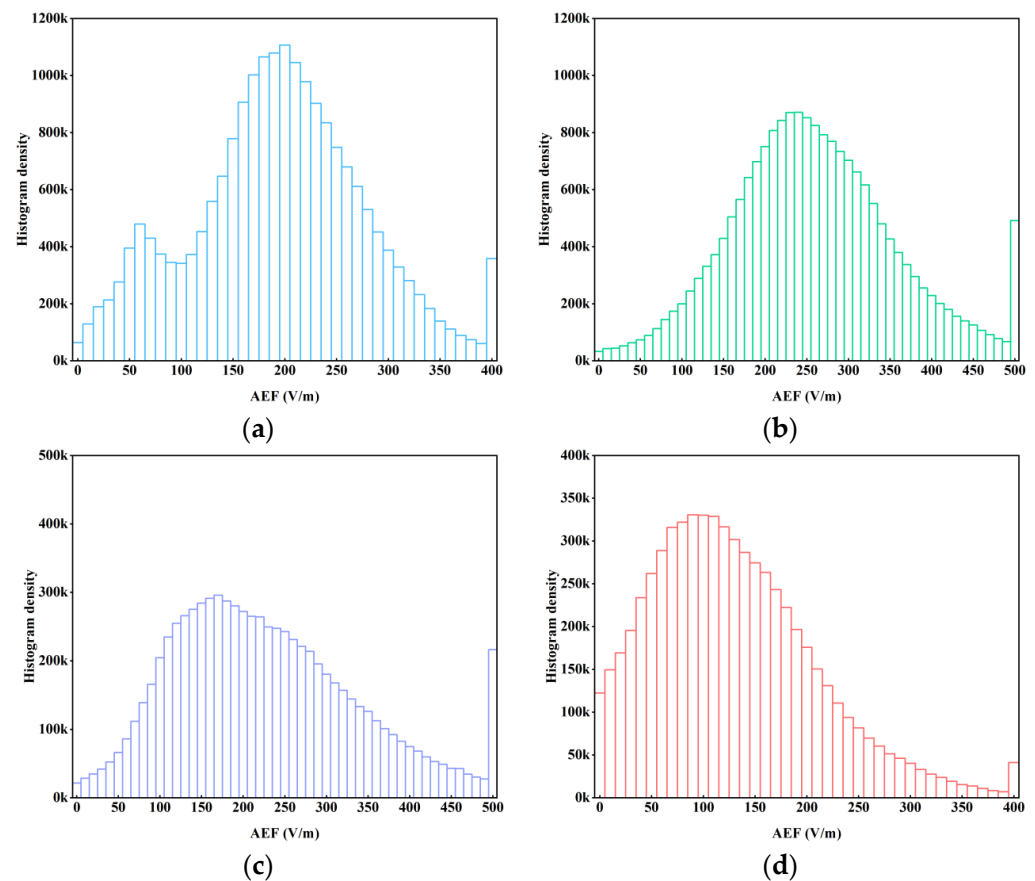


Figure 4. Histogram of fair-weather AEF values at CX, MD, LF, and DL Stations in 2022 (the interval is 10 V/m) (a–d).

Based on Figure 4, despite the differences among them, all AEF distributions adhered to the Maxwell distribution. A comparison of the four panels reveals that the AEF distributions at MD Station and LF Station were broader than the other two stations, aligning with the findings in Figure 3. The AEF range corresponding to the maximum histogram density varied: for CX Station, it was 200–210 V/m; MD Station had the largest range at 240–250 V/m; for LF Station, it was 170–180 V/m; and DL Station had the smallest range at 90–100 V/m.

The daily variations at CX, MD, LF, and DL Stations were averaged to derive the total fair-weather average AEF variation curve, with the mean AEF value set as 100% for all four stations, as depicted in Figure 5. In Figure 5, the vertical axis illustrates the percentage of the AEF value relative to the mean AEF. The blue curve signifies the percentage curve of the average fair-weather AEF daily variation at CX Station, the green curve represents MD Station, the red curve corresponds to LF Station, and the brown curve represents DL Station. The Carnegie curve is indicated by the purple dashed curve.

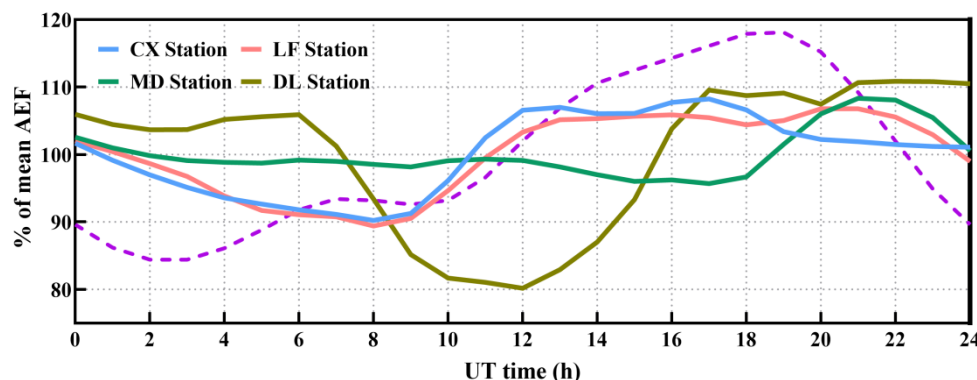


Figure 5. Average diurnal variation curve of fair AEF at CX (blue), MD (green), LF (pink), and DL (brown) Stations in 2022 (vertical axis represents the percentage of AEF value/mean AEF, and the purple dashed curve is the “Carnegie Curve”).

In Figure 5, the fair-weather AEF daily variation curve at MD Station was the flattest, with fluctuations occurring only during 18–24 UT. The AEF daily variation curves at CX Station and LF Station on fair days exhibited similarities, featuring a valley around 8 UT and a peak around 17 UT. The most pronounced changes in the daily variation curve were observed at DL Station, characterized by a singular valley at 12 UT and a single peak at 23 UT. The differences in fluctuation for CX Station, MD Station, LF Station, and DL Station were 44.5 V/m (21% of mean AEF), 47.4 V/m (18% of mean AEF), 37.9 V/m (20% of mean AEF), and 80.5 V/m (39% of mean AEF), respectively. Notably, only the AEF daily variation curve at DL Station fluctuated more dramatically than the Carnegie curve.

Upon comparing the fair-weather average AEF variation curves for these four stations with the Carnegie curve, all four AEF daily variation curves followed a “single valley, single peak” pattern despite their distinct shapes. They deviated from the Carnegie curve, exhibiting different times corresponding to peaks and valleys. The curves at CX Station and LF Station shared similarities with the Carnegie curve. Furthermore, their peaks corresponded to different UT times, likely linked to convective processes associated with sunrise and sunset. The average fair-weather AEF values for CX Station, MD Station, LF Station, and DL Station were 214 V/m, 266 V/m, 193 V/m, and 206 V/m, respectively, slightly exceeding the mean value of the Carnegie curve.

4. Conclusions and Discussion

Based on the findings presented in the figures above, the conclusions can be summarized as follows:

1. The average fair-weather AEF values for CX Station, MD Station, LF Station, and DL Station in 2022 are slightly higher than the average AEF of the Carnegie curve. This discrepancy is primarily attributed to the high altitude of these four stations, where the AEF is significantly amplified due to the compression of the AEF isopotential at high altitudes [29]. Another potential factor that could contribute to the differences is that the AEF sensors at these four stations were calibrated in the laboratory, not at the observation sites, which may introduce errors.
2. All four average daily fair AEF variation curves exhibited a “single valley, single peak” pattern, corresponding to their considerable distance from industrial areas. Diurnal variations in electric fields closer to industrial areas tend to be more complex, exhibiting double peaks, double valleys, or even multiple peaks and valleys [29].
3. Despite the short distance of only a few tens of kilometers between these four stations, the uneven terrain surrounding each station introduces differences in their sunrise and sunset times. Peaks and valleys in the AEF curves corresponded to different UT times, likely linked to convective processes arising due to sunrise and sunset.

4. The fair-weather average AEF variation curves for CX Station, MD Station, and LF Station in 2022 displayed smoother fluctuations than the Carnegie curve. This smoothness can be attributed to local effects.

In conclusion, a quadrilateral AEF monitoring network, encompassing CX Station, MD Station, LF Station, and DL Station, was established to conduct a detailed examination of the near-surface atmospheric electrostatic environment in the Yunnan region. The AEF data collected and analyzed for these four stations in 2022 contributes to further research on the relationships between the AEF and earthquakes and solar activities, leveraging the advantages of the quadrilateral AEF monitoring network.

Author Contributions: W.L. processed and analyzed the data, and prepared the original draft with contributions from all authors. Z.S., Z.Y. and Z.M. were responsible for the discussions. All authors have read and agreed to the published version of the manuscript.

Funding: This research was supported by the Scientific Instrument Developing Project of the Chinese Academy of Sciences (No. YJKYYQ20190008), National Key R&D Programme of China (Nos. 2018YFA0404201 and 2018YFA0404202), the Strategic Pioneer Program on Space Science, Chinese Academy of Sciences (No. XDA15016300), and the Strategic Priority Research Program of the Chinese Academy Science (Grant No. XDA17010303).

Institutional Review Board Statement: Not applicable.

Informed Consent Statement: Not applicable.

Data Availability Statement: The datasets used or analyzed during the current study are available from the corresponding author upon reasonable request. The data are not publicly available due to privacy.

Acknowledgments: The authors acknowledge the researchers involved in the atmospheric electric field observations.

Conflicts of Interest: The authors declare no conflicts of interest.

References

1. Dongpu, X. *Atmospheric Electric Field Characteristics Analysis and Lightning Warning Research*; Nanjing University of Information Engineering: Nanjing, China, 2012.
2. Zhixiang, X. *Atmospheric Electric Field Data Analysis and Application Research Based on Autoregressive Model and Machine Learning*; Nanjing University of Information Engineering: Nanjing, China, 2021.
3. Choudhury, A.; Guha, A.; De, B.K.; Roy, R. A statistical study on precursory effects of earthquakes observed through the atmospheric vertical electric field in northeast India. *Ann. Geophys.* **2013**, *56*, R0331.
4. Hao, J.G.; Pan, H.W.; Mao, G.M.; Zhang, Y.F.; Tang, T.M.; Li, R.D.; Li, S. Anomaly of quasi-static electric field and earthquake—Exploration of a reliable earthquake precursor. *Seismol. Geomagn. Obs. Res.* **2000**, *21*, 3–166. (In Chinese)
5. Korsunova, L.P.; Khegai, V.V.; Mikhailov, Y.M.; Smirnov, S.E. Regularities in the manifestation of earthquake precursors in the ionosphere and near-surface atmospheric electric fields in Kamchatka. *Geomagn. Aeron.* **2013**, *53*, 227–233. [[CrossRef](#)]
6. Li, Y.D.; Zhang, L.; Zhang, K.; Jin, X.B. Research on the Atmospheric Electric Field Abnormality near the Ground Surface before “5.12” Wenchuan Earthquake. *Plateau Mt. Meteorol. Res.* **2017**, *37*, 49–53.
7. Mikhailova, G.A.; Mikhailov, Y.M.; Kapustina, O.V.; Smirnov, S.E. Effects of thunderstorm activity in power spectra of the electric field in the near-surface atmosphere at Kamchatka. *Geomagn. Aeron.* **2010**, *50*, 814–823. [[CrossRef](#)]
8. Smirnov, S. Association of the negative anomalies of the quasistatic electric field in atmosphere with Kamchatka seismicity. *Nat. Hazards Earth Syst. Sci.* **2008**, *8*, 745–749. [[CrossRef](#)]
9. Hao, J.G.; Pan, H.W.; Li, D.R. Regional features of atmospheric electric field anomalies before earthquakes. *Earthquake* **1993**, *6*, 48–54.
10. Omori, Y.; Nagahama, H.; Kawada, Y.; Yasuoka, Y.; Ishikawa, T.; Tokonami, S.; Shinogi, M. Perseismic alternation of atmospheric electrical conditions due to anomalous radon emanation. *Phys. Chem. Earth* **2009**, *34*, 435–440. [[CrossRef](#)]
11. Chen, T.; Zhang, X.X.; Zhang, X.M.; Jin, X.B.; Wu, H.; Ti, S.; Li, R.K.; Li, L.; Wang, S.H. Imminent estimation of earthquake hazard by regional network monitoring the near surface vertical atmospheric electrostatic field. *Chin. J. Geophys.* **2021**, *64*, 1145–1154.
12. Jin, X.; Zhang, L.; Bu, J.; Qiu, G.; Ma, L.; Liu, C.; Li, Y. Discussion on anomaly of atmospheric electrostatic field in Wenchuan Ms8.0 earthquake. *J. Electrostat.* **2020**, *104*, 103423. [[CrossRef](#)]
13. Bingyuan, L. *The Research on the Application of the Data of Atmospheric Electric Field in Lightning Warning*; University of Electronic Science and Technology: Chengdu, China, 2012.

14. Troshichev, O.A.; Frank-Kamenetsky, A.; Burns, G.; Füllekrug, M.; Rodger, A.; Morozov, V. The relationship between variations of the atmospheric electric field in the southern polar region and thunderstorm activity. *Adv. Space Res.* **2004**, *34*, 1801–1805. [[CrossRef](#)]
15. Whipple, F.J.W. Modern views on atmospheric electricity. *Q. J. R. Meteorol. Soc.* **2010**, *64*, 199–222. [[CrossRef](#)]
16. Wilson, C. Investigations on Lightning Discharges and on the Electric Field of Thunderstorms. *Philos. Trans. R. Soc. Lond.* **1921**, *221*, 73–115. [[CrossRef](#)]
17. Li, R.K.; Chen, T.; Luo, J.; Zhou, L.M.; He, Z.H.; Wang, C.Q.; Sun, Y.Q. Enhancement of High Energy Electron Fluxes and Variation of Atmospheric Electric Field in the Antarctic Region. *Chin. J. Space Sci.* **2016**, *36*, 40–48. [[CrossRef](#)]
18. Shumilov, O.I.; Kasatkina, E.A.; Frank-Kamenetsky, A.V. Effects of extraordinary solar cosmic ray events on variations in the atmospheric electric field at high latitudes. *Geomagn. Aeron.* **2015**, *55*, 650–657. [[CrossRef](#)]
19. Tacza, J.; Raulin, J.P.; Mendonca, R.R.S.D.; Makhmutov, V.S.; Marun, A.; Fernandez, G. Solar Effects on the Atmospheric Electric Field During 2010–2015 at Low Latitudes. *J. Geophys. Res. Atmos.* **2018**, *123*, 11970–11979. [[CrossRef](#)]
20. Anisimov, S.V.; Shikhova, N.M.; Kleimenova, N.G. Response of a magnetospheric storm in the atmospheric electric field of the midlatitudes. *Geomagn. Aeron.* **2021**, *61*, 180–190. [[CrossRef](#)]
21. Harrison, R.G.; Nicoll, K.A.; McWilliams, K.A. Space weather driven changes in lower atmosphere phenomena. *J. Atmos. Sol.-Terr. Phys.* **2013**, *98*, 22–30. [[CrossRef](#)]
22. Harrison, R.G. The Carnegie Curve. *Surv. Geophys.* **2013**, *34*, 209–232. [[CrossRef](#)]
23. Bhattacharyya, T.; Chatterjee, A.; Das, S.K.; Singh, S.; Ghosh, S.K. Study of fair weather surface atmospheric electric field at high altitude station in Eastern Himalayas. *Atmos. Res.* **2020**, *239*, 104909. [[CrossRef](#)]
24. Li, L.; Chen, T.; Ti, S.; Wang, S.H.; Song, J.J.; Cai, C.L.; Liu, Y.-H.; Li, W.; Luo, J. Fair-Weather Near-Surface Atmospheric Electric Field Measurements at the Zhongshan Chinese Station in Antarctica. *Appl. Sci.* **2022**, *18*, 9248. [[CrossRef](#)]
25. Li, L.; Chen, T.; Ti, S.; Wang, S.; Cai, C.; Li, W.; Luo, J. Surface atmospheric electric field variability on the Qinghai-Tibet Plateau. *Meteorol. Atmos. Physics.* **2023**, *135*, 17. [[CrossRef](#)]
26. Wu, T.; Lv, W.; Liu, X. Characteristics of atmospheric electric field near the earth's surface under different weather conditions in Beijing. *J. Appl. Meteorol. Sci.* **2009**, *20*, 394–401.
27. Harrison, R.G.; Nicoll, K.A. Fair weather criteria for atmospheric electricity measurements. *J. Atmos. Sol. Terr. Phys.* **2018**, *179*, 239–250. [[CrossRef](#)]
28. Bennett, A.J.; Harrison, R.G. Atmospheric electricity in different weather conditions. *Weather* **2007**, *62*, 277–283. [[CrossRef](#)]
29. Sun, J. *Basics of Atmospheric Electricity*; Meteorological Press: Beijing, China, 1987.

Disclaimer/Publisher's Note: The statements, opinions and data contained in all publications are solely those of the individual author(s) and contributor(s) and not of MDPI and/or the editor(s). MDPI and/or the editor(s) disclaim responsibility for any injury to people or property resulting from any ideas, methods, instructions or products referred to in the content.